View metadata, citation and similar papers at core.ac.uk
brought to you by CORE
provided by NASA Technical Reports Server

6P 324750

N95- 14526

OSCILLATORY THERMOCAPILLARY CONVECTION

Michael R. Mundrane and Abdelfattah Zebib
Department of Mechanical and Aerospace Engineering
Rutgers University
Piscataway, NJ 08855-0909

ABSTRACT

We study thermocapillary and buoyant thermocapillary convection in rectangular cavities with aspect ratio $A = 4$ and $\mathbf{Pr} = 0.015$. Two separate problems are considered. The first is combined buoyant thermocapillary convection with a nondeforming interface. We establish neutral curves for transition to oscillatory convection in the $\mathbf{Re} - \mathbf{Gr}$ plane. It is shown that while pure buoyant convection exhibits oscillatory behavior for $\mathbf{Gr} > \mathbf{Gr}_{cr}$ (where $\mathbf{Gr}_{cr}$ is defined for the pure buoyant problem), pure thermocapillary convection is steady within the range of parameters tested. In the second problem, we consider the influence of surface deformation on the pure thermocapillary problem. For the range of parameters considered, thermocapillary convection remained steady.

INTRODUCTION

Understanding and controlling oscillatory thermocapillary convection is very important to material processing in microgravity. Thermocapillary flows, driven by tangential shear associated with temperature induced surface tension gradients at a free surface, are a primary mechanism for convection under reduced gravity. While steady convection reduces the diffusional boundary layer at the solidification interface during crystal growth, and thus is generally beneficial, unsteady convection has a negative impact on crystal morphology, rendering the resulting product unusable.

A number of recent numerical studies have predicted transitions in the pure thermocapillary problem for both small and large $\mathbf{Pr}$ [1, 2, 3] while others [4, 5, 6, 7] could only predict steady states. Calculations which included buoyant affects in addition to thermocapillary affects have also been performed and displayed both steady and unsteady behavior [8, 9].

Because the buoyant problem is well understood, an indirect approach is utilized in the present work to shed light on the behavior of the thermocapillary problem. We specifically consider the behavior of the Hopf bifurcation, which clearly exists in the pure buoyant case ($\mathbf{Re} = 0$) but subsequently disappears under pure thermocapillary conditions ($\mathbf{Gr} = 0$). Numerically estimated neutral stability curves are presented in a $\mathbf{Gr} - \mathbf{Re}$ parameter space and thereby the fate of the Hopf bifurcation under the influence of thermocapillary forces is displayed. We analize the transfer of energy between the steady and oscillatory components of the flow to identify the driving mechanism for time dependent flow.

We also consider pure thermocapillary convection in a cavity and incorporate a deforming interface using two different approaches. The first approach is an asymptotic expansion with respect to the small parameter $\mathbf{Ca}$. The $O(1)$ and $O(\mathbf{Ca})$ solutions are obtained. The second approach employs a linearized free surface condition.

MATHEMATICAL MODEL

The physical model consists of a rectangular calculation domain with aspect ratio $A = width/height$ (see Figure 1). There is a free surface ($y = H$) across which no mass transport takes place. A driving temperature difference ($T_h - T_c$) is imposed in the x direction by assuming differentially heated side walls and adiabatic conditions are assumed at the two remaining boundaries. The fluid is Boussinesq and the surface tension is assumed to be a monotonic, weak function of temperature $\sigma = \sigma_r - \gamma(T^* - T_r)$ where $\gamma = -d\sigma/dT^*$. The superscript on T indicates a dimensional quantity and T_r is a reference temperature. Other nondimensional parameters are the Prandtl ($\mathbf{Pr} = \nu/\alpha$), Reynolds ($\mathbf{Re} = \gamma T_r L/\mu\nu$), Grashof ($\mathbf{Gr} = g\beta T_r L^3/\nu^2$), Marangoni ($\mathbf{Ma} = \mathbf{RePr}$) numbers. The symbols ν and μ represent the kinematic and dynamic viscosities respectively. In addition, the Capillary number ($\mathbf{Ca} = \gamma T_r/\sigma_r$) provides some measure of the surface deflection in response to thermocapillary induced stresses. This parameter is small in value and in the limit $\mathbf{Ca} \rightarrow 0$, the free surface is flat.

For the combined problem, scales $L = H$, $T_r = (T_h - T_c)/A$, $\mathbf{Gr}\,\nu/L$, L^2/ν, and $\mathbf{Gr}\,\nu\mu/L^2$ are applied to length, temperature, velocity, time, and pressure respectively and permit the influence of both buoyant and thermocapillary effects [10, 11]. Scales $L = H$, $T_r = T_h - T_c$, $\gamma T_r/L$, L^2/ν, and $\gamma\, T_r/L$ are applied to length, temperature, velocity, time, and pressure respectively for the thermocapillary problem.

Free surface deformation is incorporated by performing an asymptotic expansion with respect to the small parameter $\mathbf{Ca}$. Grouping terms of $O(1)$ and terms of $O(\mathbf{Ca})$ yields a nonlinear and a linear system of equations and boundary conditions representing a leading order solution and a correction, respectively. A second approach is to linearize the free surface boundary conditions by performing an expansion with respect its equilibrium position [12].

RESULTS

Based on numerous computations at carefully selected parameter values, neutral stability curves (see Figure 2) have been generated in the $\mathbf{Re}-\mathbf{Gr}$ parameter space. The displayed curves represent both $\mathbf{Pr}$ and aspect ratio dependence for the Hopf bifurcation of the combined buoyant and thermocapillary problem. It can be seen that the generated curves do not intersect the $\mathbf{Gr} = 0$ line at any point. This has also been confirmed by calculations performed for $\mathbf{Pr} = 0$. The results are consistent with both steady and unsteady calculations performed by Hadid and Roux [9]. The neutral curve is shifted upwards (a stabilized flow) if either the aspect ratio is decreased or if the Prandtl number is increased.

Insight into the mechanism of instability can be obtained by computing the production and dissipation of energies for a given disturbance [13]. We assume that the flow field can be decoupled into a time averaged $\mathbf{U}$ calculated in a protracted fashion over many cycles and a perturbation $\mathbf{u}'$ extracted directly as the instantaneous difference between the actual and the "base" flow field given by $\mathbf{U}$. The analyses are performed for the limiting case of $\mathbf{Pr} = 0$ which prescribes a conduction profile and thereby eliminates the small contributions of the fluctuating temperature field present with small but nonzero $\mathbf{Pr}$. The vector dot product of the perturbation velocity and the momentum equation is integrated over the calculation domain to define the energy and thus obtain the Reynolds-Orr energy equation $\dot{\mathbf{K}}$ in terms of production P and dissipation D in the form

$$\int \dot{\mathbf{K}} d\mathbf{x} = \int \mathbf{Gr}\,\mathbf{P} d\mathbf{x} - \int \mathbf{D} d\mathbf{x}$$

This equation evaluates the net transfer of energy between the base flow and the perturbation. If the transfer is positive/negative, then the flow is unstable/stable to the perturbation.

Stream function contours for the averaged flow field and local rate of change of kinetic energy for reinforcing and opposing thermocapillarity, are indicated in Figures 3 and 4 respectively. They correspond to the same $\mathbf{Pr}$ and $\mathbf{Gr}$ with selected $\mathbf{Re}$ such that they are near the respective sides of the the neutral curve. For the reinforcing case (Figure 3) the flow consists of the buoyancy dominated clockwise corotation. Net

production which is positive, and thus representative of a transfer of energy between the underlying base flow and the unsteady perturbation flow, is present in the shear region between the two corotating cells and in the region where the cold wall cell interacts with the lower adiabatic boundary. In the opposing case (Figure 4) The base flow is seen to be separated into two distinct counter rotating cells. The lower one contains buoyancy driven clockwise corotating cells while the surface thermocapillary cells are counterclockwise and corotating. The regions of net energy transfer to the perturbation flow exist in the the shear region between the buoyancy driven corotating cells and also in the high shear region at the free surface where the buoyant cell interacts with the opposing thermocapillary surface near the hot corner. As the neutral stability curve is approached, the buoyant cell is pushed downwards into the cavity and this reduces its interaction with the free surface.

The indicated plots for energy production are not time invariant. The perturbation velocities u'_x and u'_y have the same period, but differ by some constant phase angle. However, the regions of intense shear for the opposing case remain the saddle point of the buoyant corotating cells and the interaction near the free surface between the thermocapillary and buoyant recirculations. For the reinforcing case, The relevant regions consist of the saddle point and the interaction between the buoyant recirculation and the lower surface. The contribution to the perturbation varies in importance through the limit cycle but remains associated with these respective regions. In both the opposing and the reinforcing case, energy transfer in the buoyant cells is reduced as the neutral stability curve is approached. Thus, the thermocapillary driven surface flow acts to diffuse energy transfer and ultimately net production is suppressed due to elimination of internal shear layers.

Thermocapillary convection with a deforming interface is shown in Figures 5 - 9, which corresponds to $\mathbf{Re} = 1000, 5000$. These figures display both the $O(\mathbf{Ca})$ and combined flow fields. The combination is performed utilizing an assumed $\mathbf{Ca} = 0.01$ which is consistent with the small parameter assumption in the original expansion $\phi \approx \phi_0 + \phi_1 \mathbf{Ca}$. The combined and the $O(1)$ flow fields are indistinguishable for these parameter values. The flow is seen to be unicellular and attracted to the cold corner. This is consistent with other work [4]. The temperature field does not deviate substantially from a conduction profile for this $\mathbf{Pr}$ and $\mathbf{Re}$. The calculated results were steady for the parameter values selected and the flow fields for the $O(1)$ and $O(\mathbf{Ca})$ calculations were of comparable orders of magnitude.

The surface deflection (see Figure 8) is nearly three times larger than that obtained for aspect ratio $A = 2$, $\mathbf{Pr} = 0.01$ and $\mathbf{Re} = 1000$ flows. However, this deflection is still $\approx 10^{-3}$ for the $\mathbf{Ca}$ utilized. Because h is very small, we also calculate the flow using linearized free surface boundary conditions. The results for the parameter values of Figure 5 are shown in Figure 6 where quantitative agreement of about 0.05% is indicated. The free surface velocities (see Figure 9) are qualitatively similar to profiles obtained using different aspect ratios. The peak surface velocity is near the cold wall for these calculations. This is consistent with the flow field profiles which indicate that the dominant circulation is attracted to the cold isothermal boundary for increasing $\mathbf{Re}$.

CONCLUSIONS

We have investigated the combined buoyant thermocapillary convection oscillatory states and attempted to understand the origin of these transitions. When $\mathbf{Gr}$ is sufficiently large to admit periodic solutions in the pure buoyant problem and when thermocapillarity acts in support of buoyancy, the effect is stabilizing as a larger $\mathbf{Gr}$ is needed for transition. When it acts in opposition it is destabilizing for small $|\mathbf{Re}|$ due to additional energy transfer to the fluctuating component at the free surface, but for larger $|\mathbf{Re}|$ the flow eventually separates into two distinct recirculations. One is buoyancy driven and the other is thermocapillary driven with opposing circulation. Thermocapillarity is ultimately stabilizing as it smooths out the internal buoyant shear layers. Furthermore, surface deflection which is small for small $\mathbf{Ca}$ is found to have no significant effect on the transition process, ie. the flow remained steady for all parameters utilized.

Our computational techniques have been validated against numerous published works, however, our

results do not agree only with Chen and Hwu [2]. Further studies should be conducted to establish a complete picture of the technologically important case of low **Pr**, microgravity convection. In particular, there appears to be no experimental results in the literature for this case.

ACKNOWLEDGMENTS

We wish to acknowledge the support of the National Aeronautics and Space Administration through Contract No. NAG3-1453, and the Pittsburgh Supercomputing Center for computational resources utilized in our work. We thank Prof. G. Homsy for helpful discussions and for providing us with a preprint of Ramanan and Homsy [13].

REFERENCES

[1] M. Ohnishi and H. Azuma. Computer simulation of oscillatory Marangoni flow. *Acta. Astronautica*, 26(8-10):685–696, 1992.

[2] J. C. Chen and F. S. Hwu. Oscillatory thermocapillary flow in a rectangular cavity. *Int. J. Heat Mass Transfer*, 36(15):3743–3749, 1993.

[3] L. J. Peltier and S. Biringen. Time-dependent thermocapillary convection in a rectangular cavity: numerical results for a moderate Prandtl number fluid. *J. Fluid Mech.*, 257:339–357, 1993.

[4] A. Zebib, G. M. Homsy, and E. Meiburg. High Marangoni number convection in a square cavity. *Phys. Fluids*, 28(12):3467–3476, 1985.

[5] B. M. Carpenter and G. M. Homsy. High Marangoni number convection in a square cavity: Part 2. *Phys. Fluids A*, 2:137–148, 1990.

[6] U. Buckle and M. Peric. Numerical simulation of buoyant and thermocapillary convection in a square cavity. *Numerical Heat Transfer, Part A*, 21:121–141, 1992.

[7] A. Liakopoulos and G. W. Brown. Thermocapillary and natural convection in a square cavity. In G. P. Neitzel and M. K. Smith, editors, *Surface Tension Driven Flows*, volume AMD-170, pages 57–74, New York, NY, Dec 1993. Winter Annual Meeting, ASME.

[8] T. L. Bergman and J. R. Keller. Combined buoyancy, surface tension flow in liquid metals. *Numerical Heat Transfer*, 13:49–63, 1988.

[9] H. B. Hadid and B. Roux. Buoyancy- and thermocapillary-driven flows in differentially heated cavities for low-prandtl-number fluids. *J. Fluid Mech.*, 235:1–36, 1992.

[10] B. M. Carpenter. *Combined buoyant-thermocapillary flow in a cavity.* PhD thesis, Stanford University, Stanford, CA, 1989.

[11] M. Mundrane and A. Zebib. Oscillatory buoyant thermocapillary flow. *Phys. Fluids A.*, 1994. submitted.

[12] M. Mundrane and A. Zebib. Marangoni convection with a deforming interface. New York, NY, Jan 1994. IMECE, ASME. submitted.

[13] N. Ramanan and G. M. Homsy. Linear stability of lid-driven cavity flow, 1994. preprint.

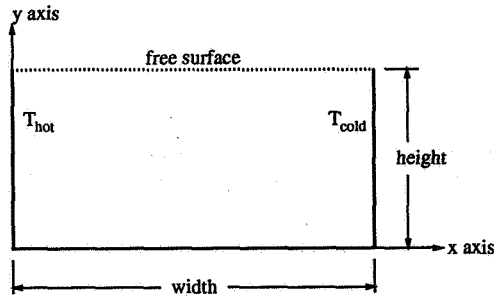

Figure 1: Physical diagram of calculation domain with solid walls as indicated. Hot and cold walls are located at $x = 0$ and $x = X_{max}$ respectively.

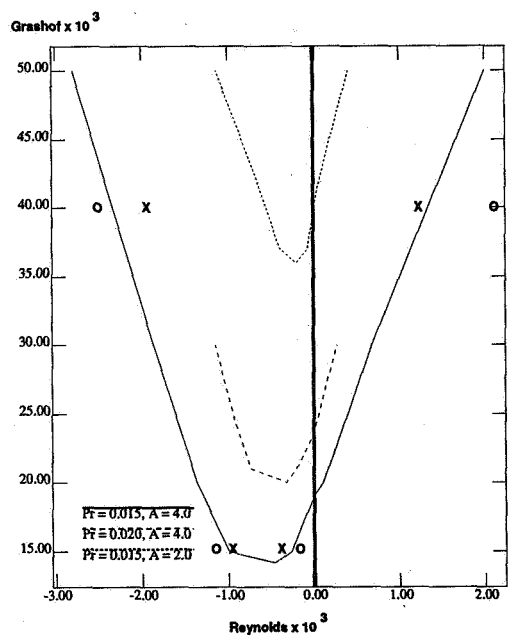

Figure 2: Neutral stability curves showing aspect ratio and **Pr** dependence. In all cases the flow is steady for **Gr** and **Re** combinations which are below the curve and unsteady for combinations which are above it. Points marked with an X (unsteady) or an O (steady) have been calculated by Hadid and Roux (1992) with aspect ratio $A = 4$ and $\mathbf{Pr} = 0.015$.

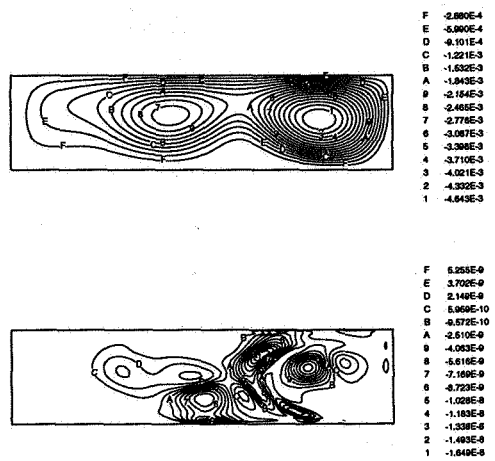

Figure 3: Averaged flow field, local production **P**, and local rate of change of kinetic energy $\dot{\mathbf{K}}$ corresponding to $\mathbf{Pr} = 0$, $\mathbf{Gr} = 20000$, and $\mathbf{Re} = 333$.

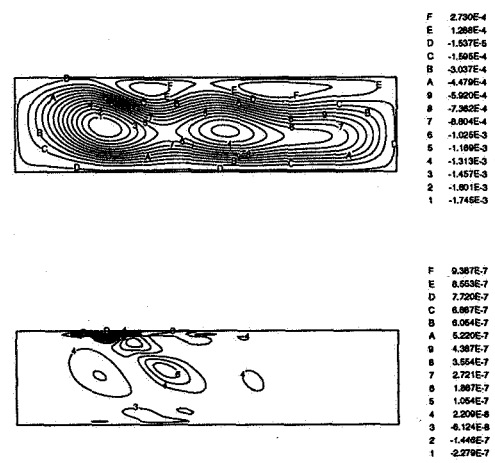

Figure 4: Averaged flow field, local production **P**, and local rate of change of kinetic energy $\dot{\mathbf{K}}$ corresponding to $\mathbf{Pr} = 0$, $\mathbf{Gr} = 20000$, and $\mathbf{Re} = -1550$.

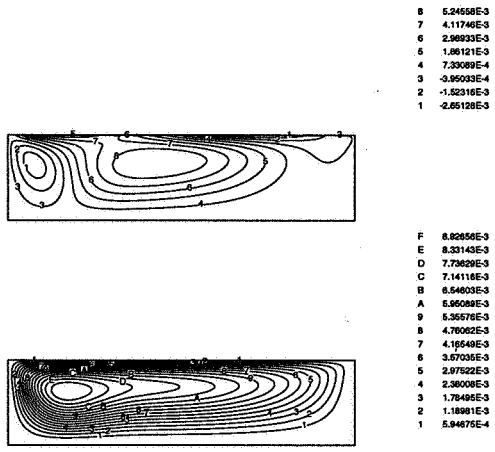

Figure 5: The upper/lower plots correspond to the $O(\mathbf{Ca})$ and combined flow fields respectively for parameter values $A = 4$, $\mathbf{Pr} = 0.015$, $\mathbf{Ca} = 0.01$, and $\mathbf{Re} = 1000$. The cold/hot isothermal boundaries are located at $x = 0, A$ respectively. The leading order flow field (not shown) is indistinguishable from the combined flow field for these parameter values.

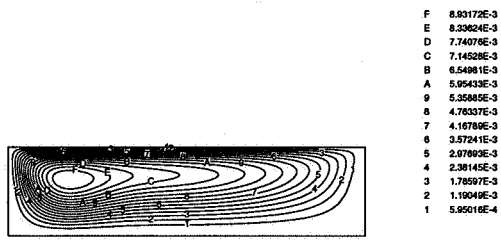

Figure 6: Complete flow field obtained utilizing the linearized approach with the same parameter values as in Figure 5. The flow fields calculated using the two different approaches differ by approximately 0.05%.

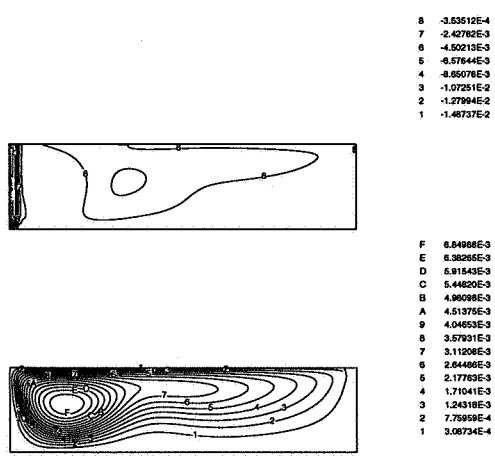

Figure 7: Similar to Figure 5, but with $\mathbf{Re} = 5000$.

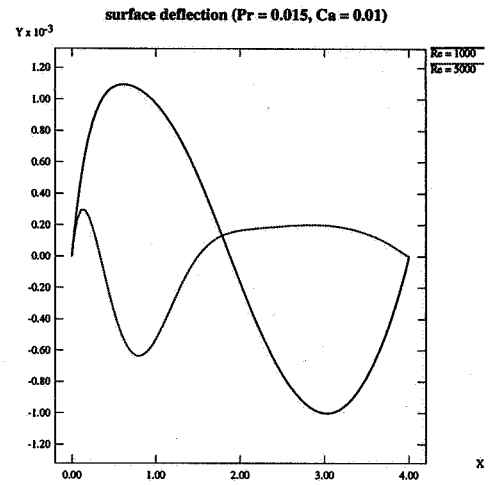

Figure 8: Free surface deflection for the same parameter values as in Figure 5 and $\mathbf{Re} = 1000, 5000$.

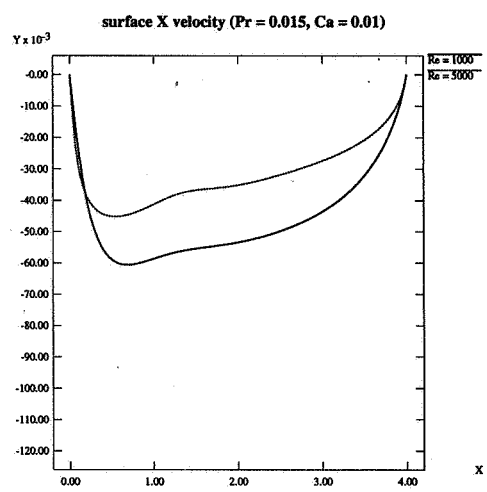

Figure 9: Free surface velocities associated with the flows of Figure 8.